High-speed dynamic 3D photoacoustic imaging of sentinel lymph node in a murine model using an ultrasound array

Liang Song, Chulhong Kim, and Konstantin Maslov
Department of Biomedical Engineering, Optical Imaging Laboratory, Washington University in St. Louis, St. Louis, Missouri 63130

K. Kirk Shung
Department of Biomedical Engineering, University of Southern California, Los Angeles, California 90089

Lihong V. Wang[a]
Department of Biomedical Engineering, Optical Imaging Laboratory, Washington University in St. Louis, St. Louis, Missouri 63130

Noninvasive photoacoustic sentinel lymph node (SLN) mapping with high spatial resolution has the potential to improve the false negative rate and eliminate the use of radioactive tracers in SLN identification. In addition, the demonstrated high spatial resolution may enable physicians to replace SLN biopsy with fine needle aspiration biopsy, and thus reduce the risk of associated morbidity. The primary goal of this study is to demonstrate the feasibility of high-speed 3D photoacoustic imaging of the uptake and clearance dynamics of Evans blue dye in SLNs. The photoacoustic imaging system was developed with a 30 MHz ultrasound array and a kHz repetition rate laser system. It acquires one 3D photoacoustic image of 166 B-scan frames in 1 s, with axial, lateral, and elevational resolutions of 25, 70, and 200 μm, respectively. With optic-fiber based light delivery, the entire system is compact and is convenient to use. Upon injection of Evans blue, a blue dye currently used in clinical SLN biopsy, SLNs in mice and rats were accurately and noninvasively mapped *in vivo* using our imaging system. In our experiments, the SLNs were found to be located at ~0.65 mm below the skin surface in mice and ~1.2 mm in rats. In some cases, lymph vessels and lymphatic valves were also imaged. The dye dynamics—accumulation and clearance—in SLNs were quantitatively monitored by sequential 3D imaging with temporal resolution of as high as ~6 s. The demonstrated capability suggests that high-speed 3D photoacoustic imaging should facilitate the understanding of the dynamics of various dyes in SLNs and potentially help identify SLNs with high accuracy. © *2009 American Association of Physicists in Medicine*.
[DOI: 10.1118/1.3168598]

Key words: dynamic 3D photoacoustic imaging, sentinel lymph node mapping, ultrasound array

I. INTRODUCTION

The sentinel lymph node (SLN) hypothesis, popularized by Morton *et al.*[1] and Giuliano *et al.*[2] in the early 1990s, states that it is sufficient to assess lymphatic metastasis by examining the first tumor-draining (sentinel) lymph node. Sentinel lymph node biopsy, based on this concept, has emerged as the standard of care in breast cancer.[3] In SLN biopsy, radioactive colloids (e.g., Tc-99m sulfur colloids) are injected preoperatively to locate the SLN with a handheld gamma probe, followed by a blue dye (e.g., methylene blue) injection to precisely locate it intraoperatively for dissection. SLN biopsy has greatly reduced unnecessary lymph node dissections and thus the risk of associated complications (e.g., lymphedema). However, it also has drawbacks:

- Up to 60 learning cases may be required to develop technical proficiency,[4] (in published results without a high number of learning cases per surgeon, up to 16% of SLNs were missed[5]).
- The false negative rate is estimated to be ~5%–10% even in experienced hands.[6,7]

- The technique involves radioactive tracer, which requires a separate injection procedure and radiation safety protections.
- Although less invasive than axillary lymph node dissection, it still has associated morbidity such as seroma formation, lymphedema, and sensory nerve injury.[8]

These drawbacks suggest that alternative strategies for SLN identification should be explored.

Ultrasound-guided fine needle aspiration biopsy has been reported as a less invasive alternative to SLN biopsy.[9,10] Unfortunately, although ultrasound can detect hypoechoic lymph nodes, it cannot distinguish the sentinel node because blue dyes have little mechanical contrast. Near infrared fluorescence imaging has been actively explored for SLN mapping.[11–13] This imaging technique performs real-time imaging capable of capturing the dynamics in SLNs.[14] However, due to the strong optical scattering in biological tissue, conventional fluorescence imaging has difficulty in identifying deep SLNs with high spatial resolution. Another challenge for fluorescence imaging is the relatively low quantum

yield of clinically approved fluorophores (e.g., ICG);[12] while quantum dots have high quantum yield, the issue of potential toxicity has to be addressed.[15]

Photoacoustic imaging combines the advantages of excellent optical absorption contrast and high ultrasonic resolution at great depths, up to a few centimeters.[16] Our group recently demonstrated that photoacoustic imaging with methylene blue dye injection can accurately identify SLNs at depths of up to 31 mm in scattering biological tissue in a rat model.[18,19] This depth is greater than the mean SLN depth (distance from the skin surface to the top surface of the SLN) of 12 ± 5 mm, which was computed from 24 ultrasound breast images randomly selected from ~200 cases taken over a 3 yr period.[17] Given the use of only conventional blue dye that is already part of the current standard of care, photoacoustic imaging is a promising technology for accurate SLN mapping, potentially capable of improving the false negative rate in SLN identification. With the demonstrated high spatial resolution, it may also have the potential to replace SLN biopsy with fine needle aspiration biopsy, and thus to reduce the risk of associated morbidity.

In photoacoustic imaging with a single-element ultrasonic transducer, the data acquisition speed is usually limited by the raster scanning.[18,19] Fortunately, this drawback can be overcome by using an ultrasound array. With a high-frequency ultrasound array, we recently developed a photoacoustic imaging system that performs 50 Hz real-time B-scan imaging and high-speed 3D imaging—one 3D image acquisition takes 1 s.[20–22] We believe that this imaging speed is highly desirable in clinics, and it is expected to facilitate the study of photoacoustic SLN mapping. In this study, we demonstrated the feasibility of SLN mapping in a murine model with our refined high-speed 3D photoacoustic imaging system. Evans blue, a blue dye used in clinical SLN biopsy,[23,24] was employed to provide the optical absorption contrast (with the peak absorption wavelength at ~620 nm, and the two half-maximum wavelengths at ~540 and 650 nm, respectively[25]) for photoacoustic imaging. In addition, the dye dynamics in SLNs were quantitatively monitored with a 3D imaging temporal resolution of as high as ~6 s.

II. MATERIALS AND METHODS

II.A. Imaging system

Figure 1 shows a schematic of the high-speed 3D photoacoustic imaging system. While the laser and the imaging head were fixed on an optical table, all the electronics were placed on a movable rack, creating a system potentially transportable to the clinics.

For photoacoustic wave excitation, a tunable dye laser (Cobra, Sirah Laser-und Plasmatechnik GmbH, Germany), pumped by a Q-switched Nd:YLF laser (INNOSLAB, Edgewave GmbH, Germany), was used. The Q-switched laser could be externally triggered up to 1 kHz without compromising pulse energy, which, together with the use of an ultrasound array and a multicore computer for parallel beamforming, was critical to achieve the high imaging speed. The
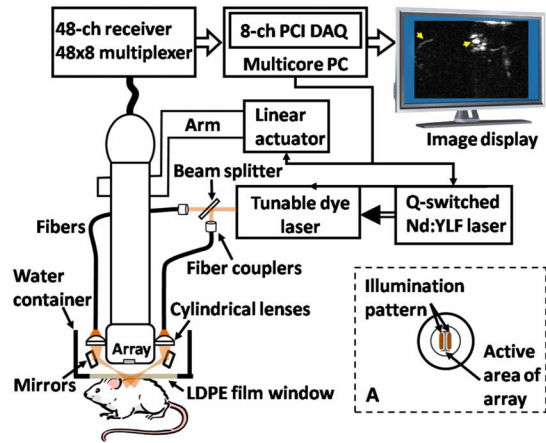

FIG. 1. Schematic of the high-speed 3D photoacoustic imaging system. Inset (a). Optical illumination pattern on the skin surface.

Q-switched laser had a pulse duration of <10 ns and a pulse energy of 11 mJ/pulse at 523 nm. The dye laser, with Pyrromethene 597 dye, had a peak output at 582 nm and a tunable range from 561 to 610 nm. The output energies from the dye laser at 584 and 600 nm—the two wavelengths used for the experiments—were ~2.5 and ~1.5 mJ/pulse, respectively.

The dye laser output was split into two beams and coupled into two 0.6-mm-core-diameter multimode optic fibers. The light beams from the output end of the optic fibers were cylindrically focused and delivered to the object to be imaged. As shown in Fig. 1 [inset (a)], dark-field laser illumination was used to reduce the photoacoustic signals from the superficial paraxial area.[26–29] The optical fluence on the skin surface of the object was estimated to be ~0.5–1.0 mJ/cm^2 per pulse, well below the ANSI recommended maximum permissible exposure (MPE) of 20 mJ/cm^2 for a single pulse. The time averaged light intensity during image acquisition was ~150–300 mW/cm^2, also below the ANSI recommended MPE calculated by $1.1t^{0.25}$ W/cm^2 (t in seconds).[30] As the ANSI safety limit for this pulse width region is dominantly based on the thermal mechanism, our compliance with the ANSI standards guarantees no thermal damage to the tissue.

We used a unique 30 MHz ultrasound array fabricated from a 2-2-piezocomposite by the NIH Resource Center for Medical Ultrasonic Transducer Technology at the University of Southern California. The array had 48 elements (82 μm $\times$ 2 mm) with 100 μm spacing. The elements were elevationally focused at 8.2 mm, providing an elevational resolution of 200 μm within the ~3.5 mm focal zone. The mean fractional bandwidth was 50% for pulse-echo operation, translating to ~70% for receiving-only operation, as used in our present photoacoustic imaging system. The axial and lateral resolutions of the system at 8 mm normal depth from the transducer surface were ~25 and ~70 μm, respectively.

While cross-sectional B-scan images were obtained by electronic beamforming using a multicore PC (Dell Precision 490 with two 2.66 GHz Quad core Xeon processors), 3D

photoacoustic images were acquired by linearly translating the array—using a linear motion actuator—in a water container (Fig. 1). The water container, with dimensions of $8 \times 5 \times 3$ cm^3 had a thin low-density polyethylene membrane window transparent to light and ultrasound. Acoustic gel was used for ultrasonic coupling between the membrane and the object. With this design, there was no direct contact between the moving imaging head and the object, minimizing potential perturbations produced by the mechanical scanning.

A high-speed (125 megasamples/s) 14-bit 8-channel DAQ card (Octopus CompuScope 8389, GaGe Applied Systems, USA) was used for data acquisition. Because of the 6:1 downmultiplexing in data acquisition, six laser shots were needed to obtain one B-scan image. The card was used as the master clock for the entire system and was programed to send trigger signals to the multiplexer control and laser. The repetition rate was set at 1 kHz, which was the highest rate that the laser could reach without degradation of pulse energy.

To obtain one 3D image, 166 B-scan frames were acquired in 996 ms, corresponding to 996 laser shots at a 1 kHz repetition rate. During the data acquisition, the array scanned at a constant speed of 10 mm/s. The speed was set so that the distance the array traveled during each B-scan was 60 μm, less than the 200 μm ultrasonic elevational focus. For sequential 3D image acquisition, the system has a temporal resolution of ~6 s, currently limited by the time for writing data to the hard drive and postbeamforming after each 3D data acquisition.

II.B. Animal model and *in vivo* imaging

Hsd:Athymic Nude mice (Harlan Laboratories, Inc., USA) weighing ~18 g and Sprague Dawley rats (Harlan Laboratories, Inc., USA) weighing ~120 g were used for the experiments. An intradermal injection of a mixture of ketamine (85 mg/kg) and xylazine (15 mg/kg) was used for initial anesthesia. For rats, the hair in the axillary region was removed with commercial hair-removal lotion before imaging. During all image acquisitions, anesthesia was maintained using vaporized isoflurane (Euthanex Co., USA). The animals were euthanized by pentobarbital overdose after experiments. All experimental animal procedures were carried out in compliance with Washington University approved protocols.

For each experiment, a control photoacoustic image of the region of interest was acquired before dye injection. Then *in situ* intradermal injection of Evans blue dye (Sigma-Aldrich Co., USA) was performed on the left forepaw pad. Photoacoustic imaging was started immediately after the dye injection. Thereafter, images were acquired every ~8 s for the initial few minutes; subsequent image acquisitions were done at longer intervals for a prolonged period, up to 1.5 h. Two laser wavelengths were used for the experiments: 584 and 600 nm. The former is close to the peak-output wavelength of the dye laser and was used to image the SLNs and blood vessels simultaneously—this wavelength also corresponds to an isosbestic point where oxy- and deoxyhemoglobin have
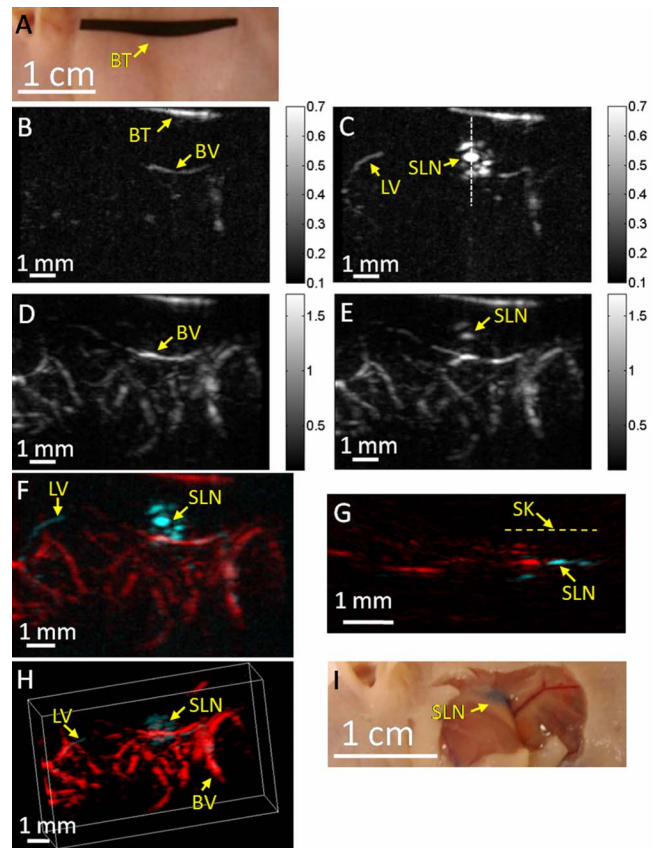
FIG. 2. Noninvasive *in vivo* photoacoustic mapping of the sentinel lymph node in a mouse. (a) Photograph taken before photoacoustic imaging. BT, black tape, was used to guide the initial positioning. (b) Control photoacoustic MAP image acquired at 600 nm laser wavelength before Evans blue injection. BV, blood vessel. The color bar represents optical absorption. (c) Photoacoustic MAP image acquired at 600 nm 8 s after Evans blue injection. SLN, sentinel lymph node. LV, lymph vessel. (d) Control photoacoustic MAP image acquired at 584 nm. (e) Photoacoustic MAP image acquired at 584 nm 8 min after Evans blue injection. (f) Composite photoacoustic MAP image. (g) Composite photoacoustic B-scan image corresponding to the dotted line in (c), showing the depth of the SLN. SK, skin surface. (h) Composite 3D photoacoustic image. (i) Photograph taken with skin removed after photoacoustic imaging.

the same optical absorption coefficient. The latter is close to the absorption peak of Evans blue and was used to image primarily the SLNs. The goal was to noninvasively identify the SLNs accurately and meanwhile capture the dye dynamics.

III. RESULTS

A mouse SLN was imaged noninvasively *in vivo* using the high-speed photoacoustic imaging system. Figure 2(a) is a photograph of the mouse taken before photoacoustic imaging, showing the axillary region. The black tape in the photograph was used to guide the initial positioning of the imaging head. Figure 2(b) is a photoacoustic control image acquired at 600 nm, shown in the form of maximum amplitude projection (MAP), which was created by projecting the maximum photoacoustic amplitudes along the depth direction to the skin surface. A few blood vessels were imaged, but the images have low contrast because of the low energy

output from the dye laser and the decreased hemoglobin absorption at this wavelength.[31] Figure 2(c) is a photoacoustic MAP image acquired at 600 nm ~8 s after injection of ~100 μg (1%, 0.01 ml) Evans blue. The SLN as well as an afferent lymph vessel are clearly seen. As 600 nm is close to the Evans blue peak absorption wavelength (620 nm), the SLN shows excellent contrast in the image. Figure 2(d) is a control photoacoustic image acquired at 584 nm, showing the subcutaneous vasculature. The spatial resolutions are 70 μm in the lateral (vertical) and 200 μm in the elevational (horizontal) directions, respectively. After Evans blue injection, both the vasculature and SLN were imaged [Fig. 2(e)]. A composite of the two photoacoustic MAP images acquired at 600 and 584 nm was obtained [Fig. 2(f)]. In this composite image, the blood vessels and dyed lymphatic system—the SLN and lymph vessel—are clearly seen with high contrast and good resolution. The distance between the top surface of the SLN and the skin surface was estimated to be 650 ± 50 μm from the composite B-scan image [Fig. 2(g)]. A composite 3D image, constructed with VolView (Kitware Inc., USA), is shown in Fig. 2(h). An invasive photograph of the same mouse, with the skin removed, was taken after photoacoustic imaging [Fig. 2(i)]. The SLN was embedded in fatty tissue, and thus difficult for naked eyes to locate precisely, even with the skin removed. The dynamic behavior of Evans blue in the SLN is shown in Fig. 3(g) (mouse 1), obtained with the aforementioned data acquisition strategy. Each data point in Fig. 3(g) was computed as the photoacoustic signal averaged over the entire SLN area in the corresponding MAP image (normalized by the temporal maximum value of the same SLN). The data points were exponentially fitted to show the change more clearly. In this case, the photoacoustic signal was observed to decrease with time from the first recorded point (8 s) and was of ~10% peak value after ~1.5 h.

Another mouse was imaged with the same scheme but with less Evans blue injection—~32 μg (0.4%, 0.008 ml). This time, a signal increase was observed within the initial ~40 s [Figs. 3(a)–3(d)], followed by a subsequent decrease [Fig. 3(e)]. A composite B-scan image [Fig. 3(f)] along the dotted line in Fig. 3(d) was obtained, showing the depth of the SLN. The quantitative dynamics were plotted in Fig. 3(g) (mouse 2), showing both a rising and a falling phase.

A rat was also imaged. After taking the control images at 600 nm [Fig. 4(a)] and 584 nm [Fig. 4(b)], ~300 μg (1%, 0.03 ml) of Evans blue was injected. In this case, the SLN as well as a lymphatic valve were identified [Fig. 4(c)]. A photoacoustic image taken at 600 nm 15 min after Evans blue injection showed a sharp signal decrease from the lymphatic valve, which became barely visible, while the SLN was still clearly imaged [Fig. 4(d)]. A composite image was formed to show the dyed lymphatic system and the blood vessels [Fig. 4(e)]. The composite B-scan image indicates that the SLN is at a depth of ~1.2 ± 0.1 mm below the skin surface [Fig. 4(f)]. The signal from the lymphatic valve decreased with time from the first recorded data, while the SLN exhibited
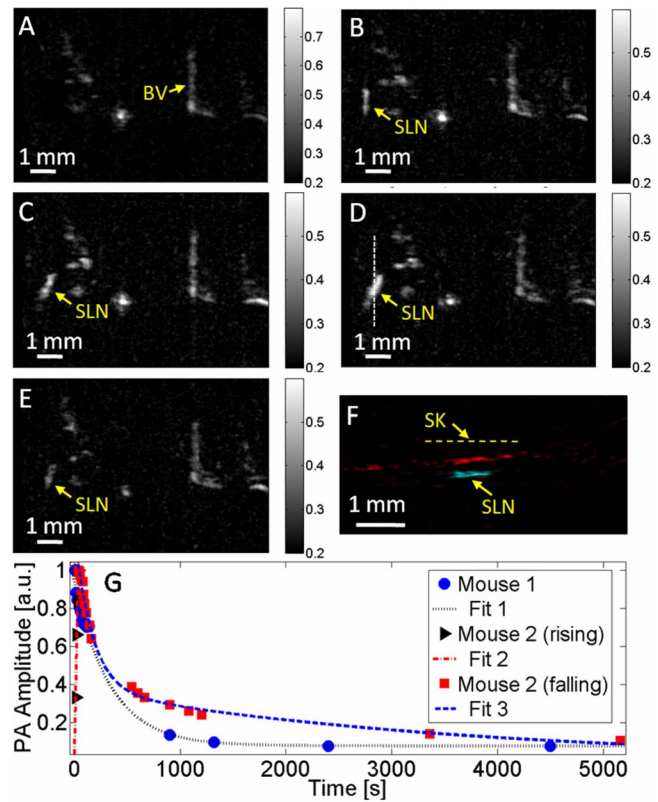
FIG. 3. Evans blue dynamics in the SLN of a mouse monitored by photoacoustic imaging. (a) Control photoacoustic MAP image in a mouse (mouse 2) acquired before Evans blue injection. BV, blood vessel. The color bar represents optical absorption. [(b)–(e)] Photoacoustic MAP images acquired at 14 s, 22 s, 38 s, and 20 min, respectively, after Evans blue injection. (f) Composite photoacoustic B-scan image corresponding to the dotted line in (d). SK, skin surface. (g) Evans blue dynamics in mice SLNs. Data points were fitted exponentially. PA, photoacoustic.

both a rising phase and a falling phase, showing the dynamics of both dye accumulation and clearance [Fig. 4(g)].

IV. DISCUSSION

Compared to pure optical imaging modalities, photoacoustic imaging is known to have high resolution at a greater imaging depth—beyond the ballistic and quasiballistic regime in scattering biological tissue—with excellent optical absorption contrast.[26,32] It is also a high-speed imaging modality by nature, with the speed fundamentally limited by the time of arrival of the photoacoustic waves, which, for example, should allow A-line acquisitions at up to 100 kHz rate at a depth of 1.5 cm. Photoacoustic imaging using a 1D ultrasound array eliminates mechanical scanning for B-scan imaging, which has led to 50 Hz real-time B-scan imaging; for 3D imaging, linear mechanical scanning is required, which, however, is still much faster than the raster scanning required by a system with a single-element ultrasonic transducer.

Currently, the high-speed photoacoustic imaging system performs real-time B-scan imaging at 50 Hz and 3D imaging of 166 B-scan frames at ~0.2 Hz, representing the highest speed in high-frequency photoacoustic imaging to our
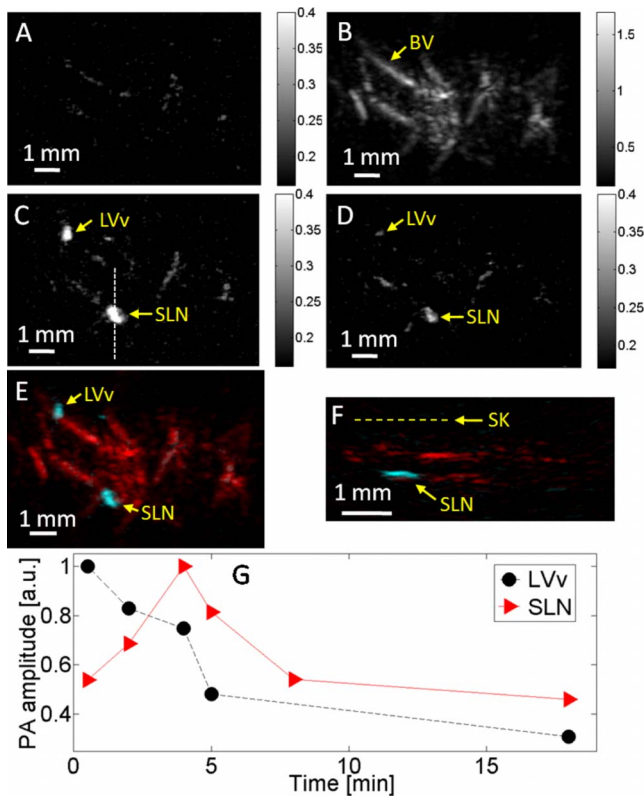
FIG. 4. Noninvasive *in vivo* photoacoustic mapping and dynamic monitoring of the sentinel lymph node in a rat. (a) Control photoacoustic MAP image acquired at 600 nm laser wavelength before Evans blue injection. (b) Control photoacoustic MAP image acquired at 584 nm, showing the subcutaneous vasculature. (c) Photoacoustic MAP image acquired at 600 nm 6 min after Evans blue injection. LVv, lymphatic valve; SLN, sentinel lymph node. (d) Photoacoustic MAP image acquired at 600 nm 15 min after Evans blue injection. (e) Composite photoacoustic MAP image. (f) Composite photoacoustic B-scan image corresponding to the dotted line in (c). SK, skin surface. (g) Evans blue dynamics in the rat lymphatic valve and SLN.

knowledge. The temporal resolution, ~ 6 s, is currently limited by the data saving and beamforming after each 3D image acquisition. It can be improved by temporarily storing all 3D data in computer memory during the entire data acquisition without beamforming, or by using a 48-channel DAQ card to eliminate the multiplexing—then one laser pulse instead of six could produce one B-scan image. We will explore both directions in the future.

In photoacoustic imaging, the spatial resolution and imaging depth are scalable with the ultrasonic frequency within the reach of photons.[32] With a 3.5 MHz single-element ultrasonic transducer and methylene blue dye (at a laser wavelength of 635 nm), photoacoustic imaging was demonstrated to be capable of imaging SLNs as deep as 31 mm in scattering biological tissue.[18,19] However, a relatively long time (20–40 min) was required to acquire one 3D image with that system. In this study, we demonstrated accurate photoacoustic SLN mapping in mice and rats, as well as the capability to quantify the dye dynamics in SLNs. As the major goal of this study was to demonstrate the feasibility of capturing the dye dynamics in SLNs with photoacoustic imaging, the choice of the dye (Evans blue) and wavelength (600 nm), limited by

the operating spectral range of our kHz repetition rate laser system, were not fully optimized for deep imaging. However, with the feasibility demonstrated in this study, we expect that a low-frequency ultrasound array (e.g., 3–5 MHz) and a high-power laser, operating at a longer wavelength (e.g., ~ 700 nm), will enable photoacoustic imaging to achieve a sufficient imaging depth (~ 30 mm), while retaining the high imaging speed. To translate the technology to the clinic, a high-speed photoacoustic imaging system with a commercial low-frequency ultrasound array is desired. Potentially, for noninvasive SLN mapping in clinics, such a system can offer advantages in precision, depth, and speed, and also provide coregistered complementary ultrasonic images.

V. CONCLUSIONS

SLNs in mice and rats were accurately mapped noninvasively *in vivo* using a high-speed 3D photoacoustic imaging system with a 30 MHz ultrasound array. The system achieved a speed for 3D photoacoustic imaging approaching 0.2 Hz, highly desirable in clinics. In addition, the dynamics of dye accumulation and clearance in the murine SLNs were quantitatively monitored with a high temporal resolution, up to 6 s. This capability should facilitate further studies to understand the dynamics of different dyes in SLNs and potentially help identify SLNs with higher accuracy.

[a])Telephone: (314) 935-6152; Fax: (314) 935-7448; Electronic mail: lhwang@biomed.wustl.edu

[1]D. L. Morton, D. R. Wen, J. H. Wong, J. S. Economou, L. A. Cagle, F. K. Storm, L. J. Foshag, and A. J. Cochran, "Technical details of intraoperative lymphatic mapping for early stage melanoma," Arch. Surg. (Chicago) **127**, 392–399 (1992).

[2]A. E. Giuliano, D. M. Kirgan, J. M. Guenther, and D. L. Morton, "Lymphatic mapping and sentinel lymphadenectomy for breast cancer," Ann. Surg. **220**, 391–398 (1994).

[3]T. Schulze, A. Bembenek, and P. M. Schlag, "Sentinel lymph node biopsy progress in surgical treatment of cancer," Langenbecks Arch. Surg. **389**, 532–550 (2004).

[4]G. Mariani, L. Moresco, G. Viale, G. Villa, M. Bagnasco, G. Canavese, J. Buscombe, H. W. Strauss, and G. Paganelli, "Radioguided sentinel lymph node biopsy in breast cancer surgery," J. Nucl. Med. **42**, 1198–1215 (2001).

[5]H. Schirrmeister, J. Kotzerke, F. Vogl, A. Buck, N. Czech, K. Koretz, G. Helm, R. Kreienberg, and T. Kuhn, "Prospective evaluation of factors influencing success rates of sentinel node biopsy in 814 breast cancer patients," Cancer Biother. Radiopharm. **19**, 784–790 (2004).

[6]K. M. McMasters, T. M. Tuttle, D. J. Carlson, C. M. Brown, R. D. Noyes, R. L. Glaser, D. J. Vennekotter, P. S. Turk, P. S. Tate, A. Sardi, P. B. Cerrito, and M. J. Edwards, "Sentinel lymph node biopsy for breast cancer: A suitable alternative to routine axillary dissection in multi-institutional practice when optimal technique is used," J. Clin. Oncol. **18**, 2560–2566 (2000).

[7]O. A. Ung, "Australasian experience and trials in sentinel lymph node

biopsy: The RACS SNAC trial," Asian J. Surg **27**, 284–290 (2004).

[8] A. D. Purushotham, S. Upponi, M. B. Klevesath, L. Bobrow, K. Millar, J. P. Myles, and S. W. Duffy, "Morbidity after sentinel lymph node biopsy in primary breast cancer: Results from a randomized controlled trial," J. Clin. Oncol. **23**, 4312–4321 (2005).

[9] S. Krishnamurthy, N. Sneige, D. G. Bedi, B. S. Edieken, B. D. Fornage, H. M. Kuerer, S. E. Singletary, and K. K. Hunt, "Role of ultrasound-guided fine-needle aspiration of indeterminate and suspicious axillary lymph nodes in the initial staging of breast carcinoma," Cancer **95**, 982–988 (2002).

[10] S. L. Koelliker, M. A. Chung, M. B. Mainiero, M. M. Steinhoff, and B. Cady, "Axillary lymph nodes: US-guided fine-needle aspiration for initial staging of breast cancer—correlation with primary tumor size," Radiology **246**, 81–89 (2008).

[11] R. Sharma, W. Wang, J. C. Rasmussen, A. Joshi, J. P. Houston, K. E. Adams, A. Cameron, S. Ke, S. Kwon, M. E. Mawad, and E. M. Sevick-Muraca, "Quantitative imaging of lymph function," Am. J. Physiol. Heart Circ. Physiol. **292**, H3109–H3118 (2007).

[12] S. Kim, Y. T. Lim, E. G. Soltesz, A. M. De Grand, J. Lee, A. Nakayama, J. A. Parker, T. Mihaljevic, R. G. Laurence, D. M. Dor, L. H. Cohn, M. G. Bawendi, and J. V. Frangioni, "Near-infrared fluorescent type II quantum dots for sentinel lymph node mapping," Nat. Biotechnol. **22**, 93–97 (2004).

[13] S. Kwon and E. M. Sevick-Muraca, "Noninvasive quantitative imaging of lymph function in mice," Lymphat. Res. Biol. **5**, 219–231 (2007).

[14] E. M. Sevick-Muraca, R. Sharma, J. C. Rasmussen, M. V. Marshall, J. A. Wendt, H. Q. Pham, E. Bonefas, J. P. Houston, L. Sampath, K. E. Adams, D. K. Blanchard, R. E. Fisher, S. B. Chiang, R. Elledge, and M. E. Mawad, "Imaging of lymph flow in breast cancer patients after microdose administration of a near-infrared fluorophore: Feasibility study," Radiology **246**, 734–741 (2008).

[15] S. Ohnishi, S. J. Lomnes, R. G. Laurence, A. Gogbashian, G. Mariani, and J. V. Frangioni, "Organic alternatives to quantum dots for intraoperative near-infrared fluorescent sentinel lymph node mapping," Mol. Imaging **4**, 172–181 (2005).

[16] K. H. Song and L. V. Wang, "Deep reflection-mode photoacoustic imaging of biological tissue," J. Biomed. Opt. **12**, 060503 (2007).

[17] J. A. Margenthaler, "Depth measurement of sentinel lymph nodes in human" (unpublished).

[18] K. H. Song, E. W. Stein, J. A. Margenthaler, and L. V. Wang, "Noninvasive photoacoustic identification of sentinel lymph nodes containing methylene blue in vivo in a rat model," J. Biomed. Opt. **13**, 054033 (2008).

[19] K. H. Song, C. Kim, C. M. Cobley, Y. Xia, and L. V. Wang, "Near-infrared gold nanocages as a new class of tracers for photoacoustic sentinel lymph node mapping on a rat model," Nano Lett. **9**, 183–188 (2009).

[20] L. Song, K. Maslov, R. Bitton, K. K. Shung, and L. V. Wang, "Fast 3-D dark-field reflection-mode photoacoustic microscopy in vivo with a 30-MHz ultrasound linear array," J. Biomed. Opt. **13**, 054028 (2008).

[21] R. J. Zemp, L. Song, R. Bitton, K. K. Shung, and L. V. Wang, "Realtime photoacoustic microscopy in vivo with a 30-MHz ultrasound array transducer," Opt. Express **16**, 7915–7928 (2008).

[22] R. J. Zemp, L. Song, R. Bitton, K. K. Shung, and L. V. Wang, "Realtime photoacoustic microscopy of murine cardiovascular dynamics," Opt. Express **16**, 18551–18556 (2008).

[23] J. Y. Bobin, C. Zinzindohoue, S. Isaac, M. Saadat, and P. Roy, "Tagging sentinel lymph nodes: A study of 100 patients with breast cancer," Eur. J. Cancer **35**, 569–573 (1999).

[24] J. Y. Bobin, C. Spirito, S. Isaac, C. Zinzindohoue, A. Joualee, M. Khaled, and O. Perrin-Fayolle, "[Lymph node mapping and axillary sentinel lymph node biopsy in 243 invasive breast cancers with no palpable nodes. The south Lyon hospital center experience]," Ann. Chir. **125**, 861–870 (2000).

[25] C. E. Patterson, R. A. Rhoades, and J. G. N. Garcia, "Evans blue-dye as a marker of albumin clearance in cultured endothelial monolayer and isolated lung," J. Appl. Physiol. **72**, 865–873 (1992).

[26] L.-H. V. Wang and H. Wu, *Biomedical Optics: Principles and Imaging* (Wiley, Hoboken, NJ, 2007).

[27] K. Maslov, G. Stoica, and L. V. Wang, "In vivo dark-field reflection-mode photoacoustic microscopy," Opt. Lett. **30**, 625–627 (2005).

[28] H. F. Zhang, K. Maslov, and L. V. Wang, "In vivo imaging of subcutaneous structures using functional photoacoustic microscopy," Nat. Protoc. **2**, 797–804 (2007).

[29] H. F. Zhang, K. Maslov, G. Stoica, and L. V. Wang, "Functional photoacoustic microscopy for high-resolution and noninvasive in vivo imaging," Nat. Biotechnol. **24**, 848–851 (2006).

[30] *Laser Institute of America, American National Standard for Safe Use of Lasers ANSI Z136.1-2000* (American National Standards Institute, Inc., New York, NY, 2000).

[31] A. Roggan, M. Friebel, K. Dorschel, A. Hahn, and G. Muller, "Optical properties of circulating human blood in the wavelength range 400–2500 NM," J. Biomed. Opt. **4**, 36–46 (1999).

[32] L. V. Wang, "Prospects of photoacoustic tomography," Med. Phys. **35**, 5758–5767 (2008).